



Non-Arrhenius diffusion in bcc titanium: Vacancy-interstitialcy model

Grigory Smirnov ^{*}

*National Research University Higher School of Economics, 123458 Moscow, Russia
and Joint Institute for High Temperatures of the Russian Academy of Sciences, 125412 Moscow, Russia*

 (Received 29 July 2020; revised 11 October 2020; accepted 30 October 2020; published 18 November 2020)

Anomalous diffusion in some bcc metals is the long-standing topic in material science. In this work, I obtain the temperature dependence of the self-diffusion coefficient in bcc titanium directly from molecular dynamics (MD) calculation. MD simulations indicate that both vacancies and self-interstitials contribute to diffusivity in bcc Ti. The resultant self-diffusion coefficient is non-Arrhenius, but shows less curvature than observed in most experiments.

DOI: [10.1103/PhysRevB.102.184110](https://doi.org/10.1103/PhysRevB.102.184110)

I. INTRODUCTION

According to the classical concepts, diffusion in normal metals mainly occurs due to the formation and migration of monovacancies [1]. The diffusion coefficient D can be expressed by the Arrhenius equation, where the activation energy Q is strongly correlated with the melting temperature T_m :

$$D = D_0 \exp\left(-\frac{Q}{k_b T}\right) = D_0 \exp\left(-\frac{\kappa T_m}{k_b T}\right). \quad (1)$$

However, the characteristic values of κ in some anomalous bcc metals (Ti, Zr, Hf, U, Ce, Gd, La, Pr, Pu, Yb) are 1.5–2 times smaller than in normal metals. The D_0 's are several orders of magnitude too small [2–4].

The strong non-Arrhenius dependence of the diffusion coefficient is additionally observed for bcc Ti and Zr, as the temperature range for their phase stability is quite large. One common feature for all anomalous metals is that the bcc phase exists only at high temperatures or pressures and is mechanically unstable at 0 K.

Two main groups of mechanisms are discussed in the literature to explain the curvature in the Arrhenius plot [2,3,5]. The first category involves extrinsic defects to explain the high diffusivity at low temperatures; - enhanced diffusion along grain boundaries or dislocations, nonequilibrium defects due to phase transitions, or extrinsic vacancies introduced by impurity atoms. The second group focuses on intrinsic defects and their properties near the melting point. This includes the formation of divacancies, self-interstitials, or metastable ω -phase nuclei. Despite considerable efforts, there is no unambiguous experimental evidence for these versions.

Modeling of diffusion in such systems also has several difficulties. The standard zero-temperature density functional theory (DFT) methods are inadequate for calculations of the defect formation and migration enthalpies and entropies. Free energy calculations of the ideal lattice are also challenging [6].

Direct calculation of the diffusion coefficient from molecular dynamics (MD) is also difficult, the characteristic values of D in anomalous metals are 10^{-14} – 10^{-11} m²/s. Even so, bcc titanium is the most suitable material for studying anomalous diffusion due to the availability of various experimental data and different interatomic potentials for MD simulations.

Non-Arrhenius diffusion of ⁴⁴Ti in bcc Ti was observed by Murdoc, Lundy, and Stansbury [7], though they could not rule out the unambiguous explanation of the anomaly. They fit the data to the sum of two exponential terms:

$$D = D_1 \exp\left(-\frac{Q_1}{k_b T}\right) + D_2 \exp\left(-\frac{Q_2}{k_b T}\right) \quad (2)$$

with $D_1 \ll D_2$. The first term matches the data at low temperatures and the second term contributes to the high-temperature region.

Walsøe de Reca and Libanati [8] obtained slightly lower values of the tracer diffusion coefficient and did not confirm the anomalous temperature behavior. Next, Köhler *et al.* [9] confirmed the Murdock results and attributed the anomaly to the formation of the ω -phase embryos with the following model:

$$D = D_0 \exp\left(-\frac{Q}{k_b T}\right) \exp\left(\frac{G_0^M T^0}{k_b T^2}\right), \quad (3)$$

where G_0^M is the free energy of vacancy migration in pure bcc lattice below a hypothetical instability temperature T^0 .

Pontau and Lazarus [10] measured the self-diffusion coefficient at three temperatures. Their data agree well with Murdock and Köhler points at low temperatures, while the high-temperature point falls well below, close to the Walsøe del Reca and Libanati curve. Pontau and Lazarus also did not directly support any model for the anomalous diffusion.

Vogl *et al.* [11] measured the elementary diffusion jump with quasielastic neutron scattering and concluded that diffusion is carried almost exclusively by atomic jumps into vacancies, and an additional 10–15% contribution of next nearest-neighbor jumps in the [100] direction via a divacancy or a dumbbell is possible.

^{*}grsmirnov@gmail.com; gsmirnov@hse.ru

Based on the *ab initio* and classical MD calculations with Ko *et al.* modified embedded atom method (MEAM) potential [12], the authors of a recent Letter [13] suggested that the migration of vacancies and the concerted migration of atoms may explain the anomalous non-Arrhenius temperature dependence of the self-diffusion coefficient in bcc Ti. The concerted migration of atoms was also observed by Belonoshko *et al.* in bcc Fe at extreme temperatures and pressures [14]. The total self-diffusion coefficient in Ref. [13] is expressed as

$$D = c_e^{\text{vac}} D^{\text{vac}} + (1 - c_e^{\text{vac}}) D_c, \quad (4)$$

where c_e^{vac} is the thermal equilibrium concentration of vacancies, D_{vac} is the diffusivity of an individual vacancy, D_c is the diffusivity in an ideal lattice without defects. However, the absolute values of the self-diffusion coefficient in their work are ten times higher than the experimental data. Good agreement between the experimental and calculated data is achieved only on the homologous temperature scale with the melting temperature $T_m = 1651$ K, which is calculated in the original paper of Ko *et al.* [12]. Recently Dickel *et al.* [15] showed that the actual T_m value for this potential is 1719 K (the experimental value is 1940 K), which worsens the agreement on the homologous temperature scale.

Kadkhodaei and Davariashtiyani [16] used the *ab initio* MD and lattice dynamics calculations to get the self-diffusion coefficient below 1600 K for bcc Ti and below 1700 K for bcc Zr. They consider vacancy-driven mechanism with temperature dependent vibration frequency and formation entropy. However, their analysis completely ignores the formation and migrations of self-interstitials, as well as influence of temperature on the migration enthalpy of vacancies.

In this paper, I use the classical MD and zero-temperature DFT simulations to show that enhanced diffusion at high temperatures is the result of self-interstitials contribution to the monovacancy mechanism. The self-diffusion coefficient is calculated in two distinct ways. The one involves the direct MD simulations in a slab geometry. The other based on calculations of the equilibrium concentration of point defects and their effective diffusivities. Both methods give consistent results and explain the long-standing problem of anomalous diffusion in bcc metals. Though the proposed model is not new and was discussed many times in the literature [3,9,17], there has been no experimental or theoretical confirmations so far. I also consider the formation of Frenkel pairs and their relation to the concerted migration, proposed in Ref. [13].

II. COMPUTATIONAL METHOD

Several classical interatomic potentials based on embedded atom method (EAM) and MEAM models have been developed for titanium and its alloys. A MEAM potential for Ti was created by Baskes and Johnson [18], and it accurately reproduces the properties of the hcp α -phase, but the bcc β -phase is unstable over the entire temperature range. The next version of this potential [19] also does not yield the hcp-bcc phase transformation. Further improvement was made by Hennig *et al.* [20], who developed the spline MEAM potential for modeling α , β , and ω phases. Ko *et al.* [12] developed MEAM potential for NiTi alloy, focusing on finite-temperature prop-

erties of different phases. Mendeleev *et al.* [17] proposed three EAM potentials for titanium, one correctly reproduce hcp-bcc transformation and melting temperature, and two other correctly describe the properties of defects in the hcp phase.

The MEAM potentials of both Hennig and Kowere were designed to correctly reproduce the hcp-bcc transition temperature. They observed the dynamic evolution of the bcc phase to calculate the phase transition temperatures. Dickel *et al.* [15] demonstrated that this method systematically underestimates the correct hcp-bcc transition temperature $T_{\text{hcp-bcc}} = 1155$ K by hundreds of degrees due to the onset of mechanical instability in the bcc phase. The free energy method [15] gives $T_{\text{hcp-bcc}} = 1720$ K, $T_m = 1882$ K for the Hennig *et al.* [20] model and $T_{\text{hcp-bcc}} = 1460$ K, $T_m = 1719$ K for the Ko *et al.* model [12].

Dickel *et al.* [15] also proposed an alternative MEAM potential, which correctly describes the thermal properties of hcp and bcc phase ($T_{\text{hcp-bcc}} = 1155$ K, $T_m = 1911$ K), but fails to predict the high-pressure ω phase. The recent many-body potential by Kartamyshev *et al.* [21] and the artificial neural-network potential by Dickel *et al.* [22] offer even higher description accuracy, but they are not available in the standard MD packages.

All MD calculations in this work are performed using the LAMMPS package [23]. The Dickel *et al.* [15] MEAM potential is chosen to describe the interaction between atoms. The details of the simulations are given in the corresponding sections. The analysis, post-processing, and visualization of the data are done using the OVITO package [24].

To additionally validate the results of MD simulations, the defect formation energies are calculated using the DFT framework in the CP2K program [25]. The Perdew-Burke-Ernzerhof approximation [26] is used to the description of exchange-correlation. The norm-conserving Hartwigsen-Goedecker-Hutter pseudopotential [27] with $3s^2 3p^6 3d^2 4s^2$ valence electronic configuration and DZVP-MOLOPT basis set for titanium are utilized. The supercell for DFT calculations contains 128 Ti atoms in the bcc phase and $4 \times 4 \times 4$ k -point mesh.

III. RESULTS

A. Self-diffusion coefficient

First, the equilibrium lattice constant of bcc Ti is determined as a function of temperature using constant pressure-temperature molecular dynamics. The simulation cell with 2000 atoms and periodic boundary conditions (PBC) in all directions is used for the simulations.

This model with PBC cannot provide the proper concentration of vacancies and interstitials, as they are bound to form only by pairs. They are not equal in real materials and can be generated by extended defects. The problem is generally solved by incorporating the vacuum layer in the simulation cell. In that case, the PBC persist in two directions, and the free surfaces in the third direction act as the sources and sinks of point defects.

The initial configuration for diffusion calculations is the ideal crystal [65 600 atoms in $40 \times 40 \times 20.5$ unit cells with (001) surface orientation] with the vacuum layer in the z

direction. The thickness of the vacuum layer is sufficient to avoid the self-interaction of the surfaces. The self-diffusion coefficient of bcc Ti is obtained from constant volume-temperature (NVT) MD calculations of the mean-squared displacements (MSD) of the bulk atoms $\langle r^2 \rangle$ during the simulation time t : $\langle r^2 \rangle = 6Dt$. Nosé-Hoover chains are used to control the temperature in MD simulations.

Calculations in the slab geometry require the separation of surface and bulk diffusion. The mobility of atoms is much higher near the free surfaces, where the thin amorphous layers are formed. There are also intermediate (sub-surface) layers, where the concentration of point defect is far from the bulk value and the diffusion of atoms is somewhat too high.

The simplest approach to this problem is purely geometric, displacements are calculated only for the atoms that were in a specific (bulk) region inside the crystal at the beginning of the simulation. But some of these atoms can move from the bulk to the surface during the simulation, the resultant self-diffusion coefficient would be overestimated.

I impose the additional constraint to overcome this problem: atoms are considered to be “bulk” if they do not leave the region between z_{\min} and z_{\max} during the whole simulation. However, some of the excluded atoms have “bulk” component in their displacements, which is completely lost during such analysis. If the value of $z_{\max} - z_{\min}$ is too small, the highly-mobile atoms are not counted and the self-diffusion coefficient is underestimated. If $z_{\max} - z_{\min}$ is too high, the displacements of atoms from the sub-surface or even surface layers shift the diffusion coefficient up.

Firstly, I determine the boundaries of the sub-surface regions measuring the convergence of point defect concentration with respect to $z_{\max} - z_{\min}$ (see below in Sec. III B). The bulk region with equilibrium concentration of point defects is located between planes with $z_{\max} = 48 \text{ \AA}$ and $z_{\min} = 18 \text{ \AA}$ at $T = 1800 \text{ K}$ and $T = 1900 \text{ K}$, and between $z_{\max} = 53 \text{ \AA}$ and $z_{\min} = 13 \text{ \AA}$ at lower temperatures. The same values of z_{\max} and z_{\min} are used for the calculations of self-diffusion, with the aforementioned time-dependent constrain.

The MSD curves at different temperatures are shown in Fig. 1 in a double logarithmic scale. The length of each MD run is chosen to obtain the linear slope of $\langle r^2 \rangle$: 100 ns for $T = 1300$ and 1400 K , 40 ns for $T = 1500 \text{ K}$, and 10 ns for higher temperatures. The diffusion process becomes normal in about 1 ns above 1600 K , the last 5 ns of the MSD curves are fitted for these temperatures. For lower temperatures, 10–100 ns calculations are necessary; the fitting is performed for the last 20 ns at 1500 K , 70 ns at 1400 K , and 60 ns at 1300 K . The fitting error is estimated as the difference of the diffusion coefficients obtained from fits over the two halves of the original fit interval. This method provides the lower estimate of the self-diffusion coefficient, as some atoms move inside the bulk region for a limited period of time and they are excluded from the analysis. However, this estimate is rather accurate, the increase of bulk thickness by 10 \AA (that is including some subsurface atoms) alters the self-diffusion coefficient only by 5%.

The results of diffusion coefficient calculations are shown in Fig. 2. The experimental results are scattered and the results from MD simulations match different sets of points: Murdock *et al.* [7] and Köhler *et al.* [9] at high temperatures, and the

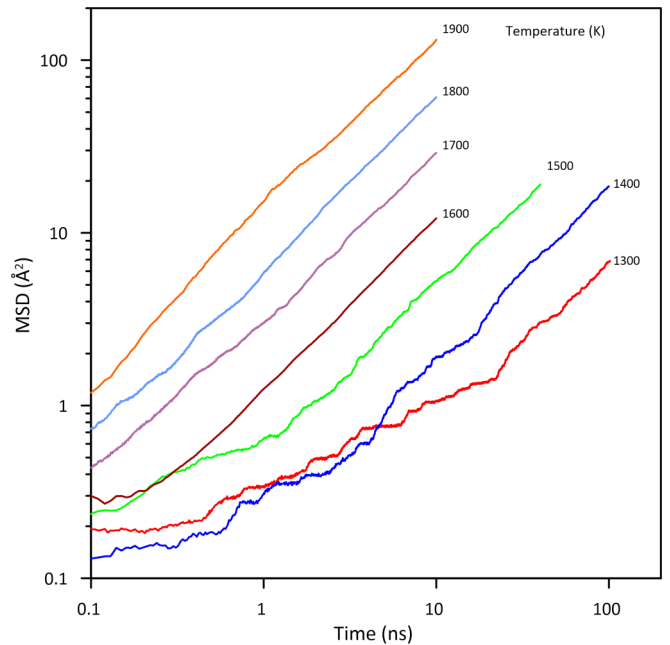


FIG. 1. Mean-squared displacements of the bulk atoms at different temperatures.

lowest values of Walsöe de Reça and Libanatti [8] at low temperatures.

The non-Arrhenius behavior of the diffusivity in MD simulations is observed without extrinsic defects: - grain boundaries, dislocations, nonequilibrium defects, and impurity atoms.

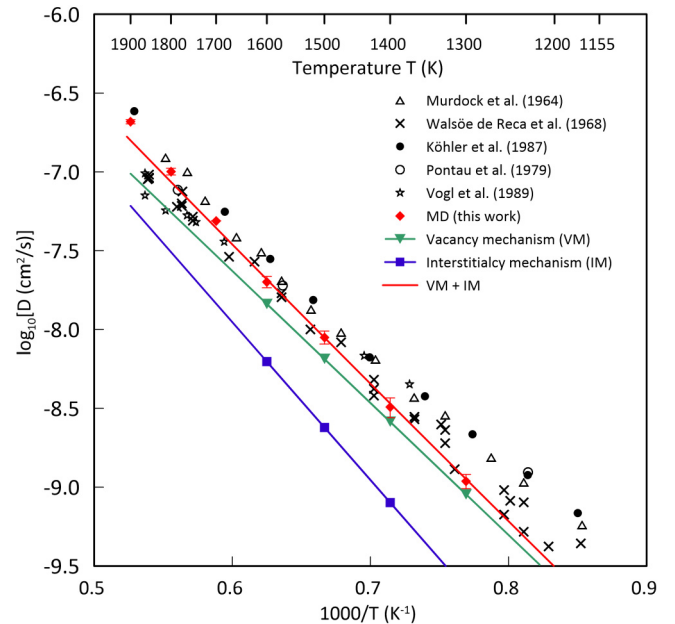


FIG. 2. Temperature dependence of the self-diffusion coefficient in bcc Ti from the experimental works [7–11] (black symbols) and the MD calculations (red diamonds, this work). Blue squares and green triangles denote the contribution of self-interstitials and vacancies respectively. Blue and green lines show the exponential fit, red line is the sum of these lines.

A contribution of divacancies and interstitials to self-diffusion is rarely considered, as their typical formation energies are too high. However, Mendelev *et al.* [17] showed that the self-interstitial formation energy in bcc Ti is smaller than the vacancy formation energy for their EAM models. The similar effect was observed in bcc Zr [28] and U [29,30].

Mendelev and Mishin [31] pointed out that the diffusion coefficient D can be also determined from the effective diffusivity D_{eff} of a single defect and the actual equilibrium concentration of defects c_e at a given temperature: $D = c_e D_{\text{eff}}$. If multiple types of defects are present in the simulation box, e.g. vacancies and self-interstitials, the total diffusion coefficient can be split into two terms:

$$D = c_e^{\text{vac}} D_{\text{eff}}^{\text{vac}} + c_e^{\text{int}} D_{\text{eff}}^{\text{int}}. \quad (5)$$

All values in Eq. (5) can be calculated directly from MD, which allows testing this two-diffusion model.

B. The mechanisms of self-diffusion

1. The concentration of point defects

The accurate determination of the total number of vacancies and self-interstitials contains many pitfalls. Normally these quantities are determined for the lattice without thermal fluctuations. There are several methods to identify them at finite temperatures.

Forsblom and Gromvall [32] used Voronoi decomposition to count the number of atoms at each Wigner-Seitz cell. Mendelev, Mishin, and Bokshtein [28,31] counted the defects by identifying the nearest lattice site for each atom. Davis, Belonoshko, and Johansson [33] proposed a stochastic optimization algorithm to locate atomic vacancies. In this work, I use Wigner-Seitz defect analysis tool in the OVITO package [24] to calculate the average number of defects inside the specific volume between z_{min} and z_{max} along the MD trajectories from the previous section. The concentration of defects is nonequilibrium in the subsurface region, and careful analysis of convergence with respect to the thickness of bulk volume is required. The convergence criterion is defined as the change in concentration by less than 1% with the change of the thickness by 4 Å. The inset in Fig. 3 shows the convergence of point defect concentration at 1400 K, the resultant boundaries of the bulk region are given in the previous section.

Calculation of the defects concentration at high temperatures contains additional difficulties. Pairs of vacancies and self-interstitials (Frenkel pairs) are created in the material through thermal fluctuations, as in superheated crystals before melting [32]. However, the crystal remains stable and no signs of melting are observed. The considered temperatures are also below the actual melting temperature for this MEAM potential (1911 K).

The Frenkel pair could form by displacement of individual atom or even atomic chain. If the pair annihilates by moving the shifted atom or chain of atoms backward, it does not contribute to the self-diffusion, but increase the appearing concentration of defects and should be excluded from the analysis. Vibrations of individual atoms could be detected and excluded by identifying the pairs of vacancies and self-interstitials within the nearest-neighbor distance. But the extended pairs (due to the vibrations of

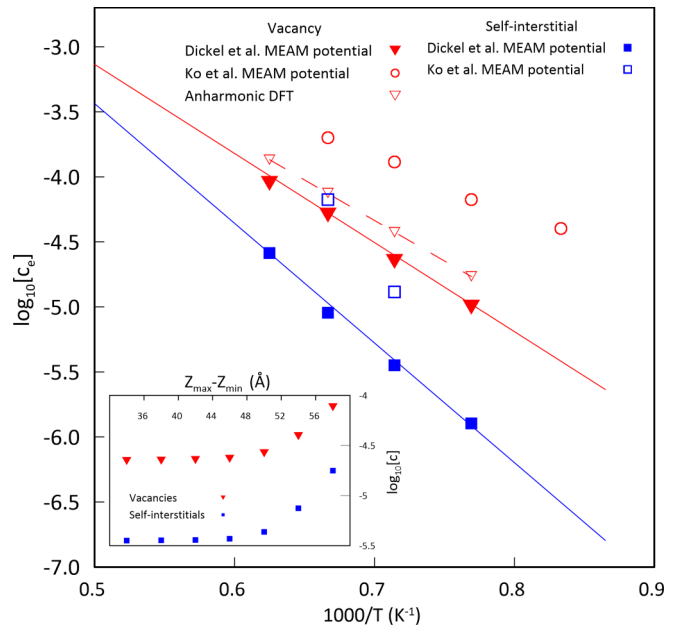


FIG. 3. The equilibrium concentration of vacancies and interstitials at different temperatures. Filled blue squares and red triangles represent the data for self-interstitials and vacancies correspondingly (this work). Open triangles show the results of anharmonic DFT calculations [16]. Circles and open squares represent the data for the Ko *et al.* [12] potential (data are taken from Ref. [13]). The straight lines denote the exponential fits for the corresponding points. The inset shows the convergence of concentrations with respect to the thickness of the bulk region at 1400 K.

atomic chains) are indistinguishable from the regular diffusing defects, as Wigner-Seitz analysis of defects relies on instantaneous atomic positions. Such extended defects inevitable enhance the concentration, but do not really participate in self-diffusion.

The Frenkel pair could also dissociate, forming the independent diffusing defects. Such events are correctly counted by Wigner-Seitz analysis, they are discussed in more details in Sec. III E.

The formation of Frenkel pairs below 1600 K occurs very rarely, all of the defects come from the surfaces, and the concentration of diffusing defects is more reliable. The high-temperature concentrations (above 1600 K) in this work are obtained by extrapolation, assuming that the Arrhenius equation for concentration is valid up to the melting point. As can be seen from Fig. 3, monovacancy is the main type of point defects in bcc Ti. Divacancies are not observed even at high temperatures. The concentration of self-interstitials is high enough near the melting point and they can contribute to the diffusion process.

The vacancy formation energy E_f^{vac} from the exponential fit of the vacancy equilibrium concentration is 1.37 eV. The corresponding self-interstitial formation energy is 1.83 eV. Anharmonic DFT calculations [16] give slightly lower value $E_f^{\text{vac}} = 1.06$ eV. The experimental data for comparison are limited. The only reported value from calorimetric measurements is $E_f^{\text{vac}} = 1.55$ eV and the corresponding concentration of vacancies at the melting point is 0.017 [34], but the

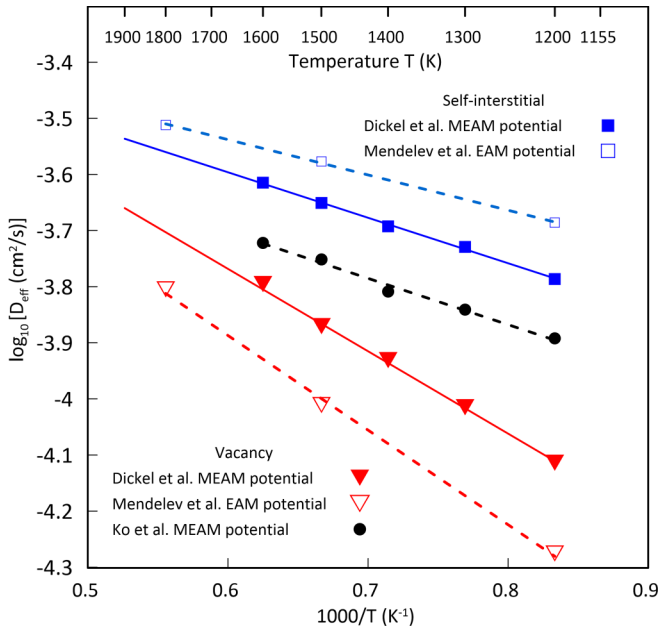


FIG. 4. The effective diffusivity as a function of temperature. Blue squares and red triangles are the data for self-interstitials and vacancies correspondingly (this work). Open symbols are for Ti1 EAM potential from Ref. [17]. Black circles show the effective diffusivity via the vacancy mechanism for the Ko *et al.* [12] potential (data are taken from Ref. [13]). The straight lines denote the exponential fits for the corresponding points.

contribution of self-interstitials is not considered in such experiments.

2. The effective diffusion coefficient

Series of NVT MD calculations with $N = 2000$ atoms and PBC are performed to calculate the effective self-diffusion coefficient D_{eff} . It can be calculated from $D_{\text{eff}} = D/c_{\text{eff}}$, where D is the actual diffusion coefficient in the simulation cell and c_{eff} is the effective concentration of defects. If the single defect is present in the simulation cell, $c_{\text{eff}} = 1/N$ and $D_{\text{eff}} = DN$.

The single defect is introduced in the ideal lattice and 10 ns MD simulation is performed. To reduce the statistical error, the diffusion coefficient is averaged by 10 independent runs. The data are well described by the Arrhenius equation at low temperatures. However, the spontaneous formation of vacancy-interstitial pairs is observed at high temperatures, as in the slab simulations. This effect does not allow to correctly calculate the self-diffusion coefficient of an individual defect. High-temperature data above 1600 K can only be obtained by extrapolation, as shown in Fig. 4.

The linear regression of $\ln(D_{\text{eff}})$ vs $1/T$ gives the defect migration energy. The resultant values for the potential of Dickel *et al.* are 0.3 eV for the vacancy migration and 0.16 eV for the self-interstitial migration. Mendeleev *et al.* [17] obtained similar values using their Ti1 EAM potential: 0.29 and 0.11 eV correspondingly. DFT calculations [16] yield the value of 0.274 eV for the vacancy migration, which is very close to these data. Sangiovani *et al.* [13] found the lower value 0.19 eV using the Ko *et al.* [12] MEAM potential. Calculations of the self-interstitial migration with this

potential give the result, which is very close to the Mendeleev data.

The effective diffusivity of the self-interstitials is 1.5–2 higher than the vacancies. That is combined with their relatively high concentration near the melting point give the observable contribution to the self-diffusion process in bcc Ti.

C. Two diffusion model

Combining the concentration of point defects and their effective diffusivity one can obtain the total self-diffusion coefficient as the sum of two terms [Eq. (2)]:

$$D[\text{cm}^2/\text{s}] = 2.49 \times 10^{-3} \exp\left(-\frac{1.66\text{eV}}{k_b T}\right) + 0.011 \exp\left(-\frac{1.99\text{eV}}{k_b T}\right). \quad (6)$$

The first term represents the contribution of vacancies and the second term represents the contribution of self-interstitials. The corresponding lines and their sum are shown in Fig. 2. At low temperature the resultant curve almost exactly coincides with the self-diffusion coefficient from the direct MD calculations. There exists a discrepancy at high temperatures, where the concentrations of defects and the effective self-diffusion coefficients are obtained by the extrapolation. Possible nonlinear temperature dependence of the defect formation and migration free energies may shift pre-exponential factors in Eq. (6) at high temperatures.

The pre-exponential factor for the vacancy mechanism is about five times lower than for the interstitial mechanism. However, the vacancy mechanism dominates in the whole temperature range due to the lower activation energy. Highly-mobile self-interstitials contribute to the diffusion even near the hcp-bcc transition temperature, where they provide about 10% to the total diffusivity.

D. Point defect formation energies from DFT calculations

The equilibrium concentration of vacancies from MD calculations agrees well with the anharmonic DFT calculations [16]. To additionally validate the formation energy of self-interstitials, I perform the series of the DFT simulations. The formation energy of a single vacancy is defined as $E_f^{\text{vac}} = E_{N-1} - \frac{N-1}{N}E_N$, where E_N is the energy of the ideal lattice with N atoms and E_{N-1} is the energy of the supercell with one vacancy. Similarly for the self-interstitial, $E_f^{\text{int}} = E_{N+1} - \frac{N+1}{N}E_N$.

As bcc Ti lattice is unstable at 0 K, the relaxation of atomic position yields the unrealistic structure. To avoid this issue, a geometric optimization is performed only for the 14 nearest atoms to the defect (two nearest shells), meanwhile the electron density optimization is performed using all atoms. The similar method was used by Beeler *et al.* [29] to calculate the defect formation energies for bcc γ -U. They also calculate the defect formation energies for bcc Mo, which is mechanically stable at 0 K, and showed that the error of the shell method does not exceed

TABLE I. The formation energy of defects (in eV) from DFT calculations.

Vacancy	1.1
$\langle 100 \rangle$ dumbbell	1.97
$\langle 110 \rangle$ dumbbell	1.76
$\langle 111 \rangle$ dumbbell	2.12
Octahedral site interstitial	2.51
Tetrahedral site interstitial	2.39

10–15%. However, it incorrectly predicts the ground state configuration of the dumbbell ($\langle 110 \rangle$ instead of $\langle 111 \rangle$).

The equilibrium lattice constant of the system is calculated by minimizing the energy with the volume of the supercell, keeping the relative positions of atoms fixed. Using the equilibrium lattice parameter, a single atom is removed (or added) to the supercell, E_{N-1} and E_{N+1} are calculated using the method described above. The resultant energies are given in Table I.

This approximate method gives the vacancy formation energy 1.1 eV very close to result from precise anharmonic DFT calculations [16] (1.06 eV). The $\langle 110 \rangle$ dumbbell configuration has the lowest formation energy 1.76 eV, which is also much lower than the typical values in bcc transition metals [35,36]. MD calculations in this work give the similar value of 1.83 eV.

E. Formation of vacancy-interstitialcy pairs

In this section, I discuss the formation of Frenkel pairs in bcc Ti at high temperatures and the concerted mechanism proposed in Ref. [13]. These defects are formed via thermal fluctuations, the effect becomes especially significant above 1600 K. The formation of vacancy-interstitialcy pair can be observed even in the ideal crystal with PBC in all directions. Most of the pairs are unstable, they annihilate after several MD steps and do not participate in the self-diffusion. But sometimes defects in the pair become fully independent and start to diffuse through the crystal. The spontaneous exchange of atoms via the formation of Frenkel was observed in bcc Zr by Willaime and Massobrio [37]. Similar observations were made by Fransson and Erhart [38]. Finally, the defects annihilate on the free surfaces or recombine with other defects in the crystal. The defects from the same pair can also recombine with each other, forming the specific closed-loop path.

The example of such process is shown in Fig. 5. Only the atoms involved in the diffusion are shown. At the initial stage, one of the atoms in the lattice is displaced from the equilibrium position, forming the self-interstitial and the vacancy [Fig. 5(a)]. Then the defects start to move in the opposite directions [Figs. 5(b) and 5(c)]. At some point they switch the course and start to “attract” each other [Figs. 5(d) and 5(e)]. Finally, they get together and recombine [Fig. 5(f)]. The trajectories of the displaced atoms form the closed-loop path. This example shows the diffusion of relatively large number of atoms for the potential of Dickel *et al.* at 1800 K. Similar pictures could be also obtained with the Ko *et al.* potential. See

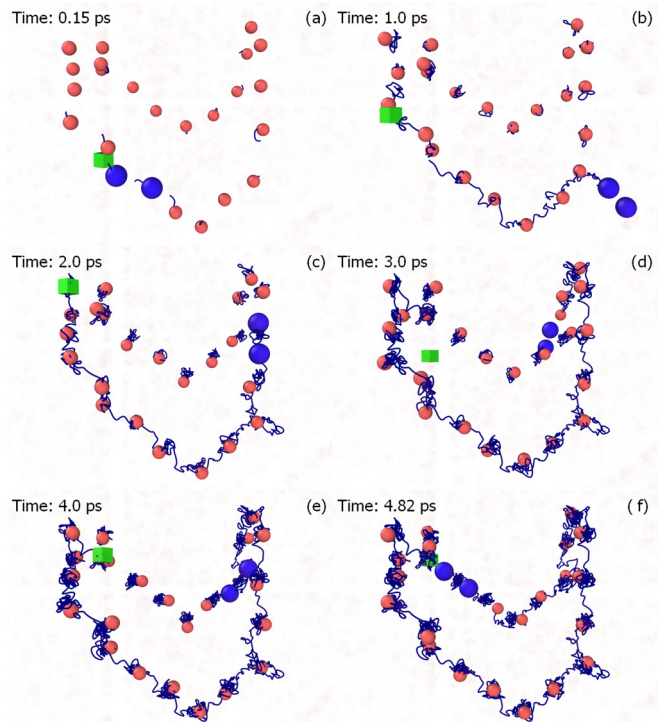


FIG. 5. The formation and recombination of the vacancy-interstitialcy pair in bcc Ti. Only the atoms with significant displacements are shown (red spheres). The green cube is the vacancy and the blue spheres represent the self-interstitial defect. The blue lines show the trajectories of diffusing atoms. The remaining atoms are semitransparent.

Supplemental Material [39] for the videos illustrating such processes. Movie S1 highlights the process shown in Fig. 5. Movies S2 and S3 demonstrate similar process for the Ko *et al.* potential at 1500 K.

Sangiovani *et al.* [13] observed similar motion of atoms and proposed the special concerted diffusion coefficient D_c associated with this mechanism. They also determined the equilibrium concentration of vacancies and interstitials at different temperatures and estimated the corresponding free energies of defect formation from the linear regression of $\ln(c_e)$ vs $1/T$: 1.0 and 3.5 eV. They concluded the resultant free energy of Frenkel pair formation 4.5 eV is too high to explain the concerted migration. However, such regression gives only the enthalpies (or energies at zero pressure) of defect formation. The formation free energy should be calculated at each temperature from the absolute values of concentrations. For example, from their absolute concentrations of defects at $T = 1500$ K one obtains $G_f^{\text{vac}} = 1.1$ eV and $G_f^{\text{int}} = 1.24$ eV. The resultant free energy of Frenkel pair formation is equal to 2.34 eV, which does not prohibit the spontaneous formation of the pairs for the Ko *et al.* potential.

IV. CONCLUSION

In summary, I show that there are two competing diffusion mechanisms in bcc Ti. In addition to the standard monovacancy mechanism, the interstitialcy mechanism contributes to self-diffusion, that has been considered improbable for a

long time. The vacancy mechanism dominates in the whole temperature range, while the self-interstitials mainly contribute to the high-temperature region. That contribution of the self-interstitials gives the slight curvature of the self-diffusion coefficient in the Arrhenius plot.

The self-interstitials in temperature-stabilized bcc Ti have the fairly low formation energy E_f^{int} compared to other stable bcc metals. The concentration of self-interstitials is close to the vacancy concentration near the melting point. This leads

to the low formation energy of Frenkel pairs, which act as an additional source of point defects.

ACKNOWLEDGMENTS

The article was prepared within the framework of the HSE University Basic Research Program. The simulations were carried out using the resources provided by the supercomputer center of NRU HSE.

-
- [1] H. Mehrer, *Diffusion in Solids*, Springer Series in Solid-State Sciences, Vol. 155 (Springer, Berlin, 2007).
- [2] N. Peterson, Diffusion in metals, in *Solid State Physics*, Vol. 22 (Academic Press, New York, 1969), pp. 409–512.
- [3] N. L. Peterson, Diffusion in the anomalous bcc metals, *Comments Solid State Phys.* **8**, 93 (1978).
- [4] C. Herzig and U. Köhler, Anomalous self-diffusion in BCC IVB metals and alloys, *Mater. Sci. Forum* **15-18**, 301 (1987).
- [5] N. Peterson, Self-diffusion in pure metals, *J. Nucl. Mater.* **69-70**, 3 (1978).
- [6] S. Kadkhodaei, Q.-J. Hong, and A. van de Walle, Free energy calculation of mechanically unstable but dynamically stabilized bcc titanium, *Phys. Rev. B* **95**, 064101 (2017).
- [7] J. F. Murdock, T. S. Lundy, and E. E. Stansbury, Diffusion of Ti^{4+} and V^{48} in titanium, *Acta Metall.* **12**, 1033 (1964).
- [8] N. Walsöe de Reça and C. Libanati, Autodifusión de titanio beta y hafnio beta, *Acta Metall.* **16**, 1297 (1968).
- [9] U. Köhler and C. Herzig, On the anomalous self-diffusion in B.C.C. titanium, *Phys. Status Solidi* **144**, 243 (1987).
- [10] A. E. Pontau and D. Lazarus, Diffusion of titanium and niobium in bcc Ti-Nb alloys, *Phys. Rev. B* **19**, 4027 (1979).
- [11] G. Vogl, W. Petry, T. Flottmann, and A. Heiming, Direct determination of the self-diffusion mechanism in bcc-titanium, *Phys. Rev. B* **39**, 5025 (1989).
- [12] W.-S. Ko, B. Grabowski, and J. Neugebauer, Development and application of a Ni-Ti interatomic potential with high predictive accuracy of the Martensitic phase transition, *Phys. Rev. B* **92**, 134107 (2015).
- [13] D. G. Sangiovanni, J. Klarbring, D. Smirnova, N. V. Skripnyak, D. Gambino, M. Mrovec, S. I. Simak, and I. A. Abrikosov, Superioniclike Diffusion in an Elemental Crystal: BCC Titanium, *Phys. Rev. Lett.* **123**, 105501 (2019).
- [14] A. B. Belonoshko, T. Lukinov, J. Fu, J. Zhao, S. Davis, and S. I. Simak, Stabilization of body-centred cubic iron under inner-core conditions, *Nat. Geosci.* **10**, 312 (2017).
- [15] D. Dickel, C. D. Barrett, R. L. Carino, M. I. Baskes, and M. F. Horstemeyer, Mechanical instabilities in the modeling of phase transitions of titanium, *Model. Simul. Mater. Sci. Eng.* **26**, 065002 (2018).
- [16] S. Kadkhodaei and A. Davariashtiyani, Phonon-assisted diffusion in bcc phase of titanium and zirconium from first principles, *Phys. Rev. Materials* **4**, 043802 (2020).
- [17] M. I. Mendeleev, T. L. Underwood, and G. J. Ackland, Development of an interatomic potential for the simulation of defects, plasticity, and phase transformations in titanium, *J. Chem. Phys.* **145**, 154102 (2016).
- [18] M. I. Baskes and R. A. Johnson, Modified embedded atom potentials for HCP metals, *Model. Simul. Mater. Sci. Eng.* **2**, 147 (1994).
- [19] Y.-M. Kim, B.-J. Lee, and M. I. Baskes, Modified embedded-atom method interatomic potentials for Ti and Zr, *Phys. Rev. B* **74**, 014101 (2006).
- [20] R. G. Hennig, T. J. Lenosky, D. R. Trinkle, S. P. Rudin, and J. W. Wilkins, Classical potential describes martensitic phase transformations between the α , β , and ω titanium phases, *Phys. Rev. B* **78**, 054121 (2008).
- [21] A. I. Kartamyshev, A. G. Lipnitskii, V. N. Saveliev, V. N. Maksimenko, I. V. Nelasov, and D. O. Poletaev, Development of an interatomic potential for titanium with high predictive accuracy of thermal properties up to melting point, *Comput. Mater. Sci.* **160**, 30 (2019).
- [22] D. Dickel, D. K. Francis, and C. D. Barrett, Neural network aided development of a semi-empirical interatomic potential for titanium, *Comput. Mater. Sci.* **171**, 109157 (2020).
- [23] S. Plimpton, Fast parallel algorithms for short-range molecular dynamics, *J. Comput. Phys.* **117**, 1 (1995).
- [24] A. Stukowski, Visualization and analysis of atomistic simulation data with OVITO—the Open Visualization Tool, *Model. Simul. Mater. Sci. Eng.* **18**, 015012 (2010).
- [25] T. D. Kühne *et al.*, CP2K: An electronic structure and molecular dynamics software package - Quickstep: Efficient and accurate electronic structure calculations, *J. Chem. Phys.* **152**, 194103 (2020).
- [26] J. P. Perdew, K. Burke, and M. Ernzerhof, Generalized Gradient Approximation Made Simple, *Phys. Rev. Lett.* **77**, 3865 (1996).
- [27] C. Hartwigsen, S. Goedecker, and J. Hutter, Relativistic separable dual-space Gaussian pseudopotentials from H to Rn, *Phys. Rev. B* **58**, 3641 (1998).
- [28] M. I. Mendeleev and B. S. Bokstein, Molecular dynamics study of self-diffusion in Zr, *Philos. Mag.* **90**, 637 (2010).
- [29] B. Beeler, B. Good, S. Rashkeev, C. Deo, M. Baskes, and M. Okuniewski, First principles calculations for defects in U, *J. Phys. Condens. Matter* **22**, 505703 (2010).
- [30] G. S. Smirnov and V. V. Stegailov, Formation free energies of point defects and thermal expansion of bcc U and Mo, *J. Phys. Condens. Matter* **31**, 235704 (2019).
- [31] M. I. Mendeleev and Y. Mishin, Molecular dynamics study of self-diffusion in bcc Fe, *Phys. Rev. B* **80**, 144111 (2009).
- [32] M. Forsblom and G. Grimvall, How superheated crystals melt, *Nat. Mater.* **4**, 388 (2005).
- [33] S. M. Davis, A. B. Belonoshko, and B. Johansson, Search-Fill: A stochastic optimization code for detecting atomic

- vacancies in crystalline and non-crystalline systems, *Comput. Phys. Commun.* **182**, 1105 (2011).
- [34] Y. Kraftmakher, Equilibrium vacancies and thermophysical properties of metals, *Phys. Rep.* **299**, 79 (1998).
- [35] D. Nguyen-Manh, A. P. Horsfield, and S. L. Dudarev, Self-interstitial atom defects in bcc transition metals: Group-specific trends, *Phys. Rev. B* **73**, 020101(R) (2006).
- [36] S. L. Dudarev and P.-W. Ma, Elastic fields, dipole tensors, and interaction between self-interstitial atom defects in bcc transition metals, *Phys. Rev. Materials* **2**, 033602 (2018).
- [37] F. Willaime and C. Massobrio, A molecular dynamics study of zirconium based on an N-Body potential: HCP/BCC phase transformation and diffusion mechanisms in the BCC-phase, *MRS Proc.* **193**, 295 (1990).
- [38] E. Fransson and P. Erhart, Defects from phonons: Atomic transport by concerted motion in simple crystalline metals, *Acta Mater.* **196**, 770 (2020).
- [39] See Supplemental Material at <http://link.aps.org/supplemental/10.1103/PhysRevB.102.184110> for the videos illustrating the formation and recombination of the Frenkel pairs.